

Optical properties of chalcogenide glasses from the system $\text{As}_2\text{Se}_3\text{-Ag}_4\text{SSe-PbTe}$

T. BABEVA^{a*}, V. VASSILEV^b, P. GUSHTEROVA^a, A. AMOVA^c, G. ALEXIEVA^d, V. STRASHILOV^d, P. PETKOVA^e

^a*Institute of Optical Materials and Technologies, Bulgarian Academy of Sciences, Acad. G. Bonchev Str., Bl. 109, 1113 Sofia, Bulgaria*

^b*University of Chemical Technology and Metallurgy, Department of Non-Ferrous Metals Metallurgy and Semiconductor Technologies, 8 Kliment Ohridski Blvd., 1756 Sofia, Bulgaria*

^c*University of Architecture, Civil Engineering and Geodesy, Hydrotechnical Faculty, Department of Physics, 1 Hristo Smirnenski Blvd., 1046 Sofia, Bulgaria*

^d*Sofia University, Faculty of Physics, Department of Solid State Physics and Microelectronics, 5 J. Bourchier Blvd., 1164 Sofia, Bulgaria*

^e*Shumen University "Konstantin Preslavsky", Faculty of Natural Sciences, Department of Experimental Physics, 115 Universitetska street, 9712 Shumen, Bulgaria*

Seven glasses from the system $\text{As}_2\text{Se}_3\text{-Ag}_4\text{SSe-PbTe}$ with appropriately chosen compositions are characterized optically through measurements of their transmittance (T) and reflectance (R) in a wide spectral range covering UV, VIS and NIR. These new chalcogenide glasses are characterized with a wide region of glass formation. For calculation of the optical properties both the Tauc-Lorentz parametrization model and the Newton-Raphson algorithm are used. Thus refractive index n , extinction coefficient k , absorption coefficient α , optical bandgap energy E_g^{opt} , and Urbach energy E_U , are obtained. Changing the composition, a considerable variation of the refractive index is achieved, the characteristic absorption edge related energies remaining practically constant. A correlation between optical parameters, glass composition and density is established and discussed.

(Received May 7, 2016; accepted April 6, 2017)

Keywords: Chalcogenide glasses, UV-VIS-NIR spectroscopy, Tauc-Lorentz model, Optical properties

1. Introduction

Chalcogenide glasses (ChGs) have attracted increasing interest in recent years from the view point of both fundamental physics and device technology and application. In contrast to traditional oxide glasses, they exhibit relatively high refractive index values ($2.0 \leq n \leq 3.7$ [1,2]) and transparency from the visible or near-infrared up to the middle infrared spectral region. As shown in [3] the IR edge is related to the chalcogen element upon which the glass is based and for Te-containing glass the transmission window is extended up to 20 microns. These features are combined with a decrease in the optical gap and increase in the electrical conductivity as compared to traditional oxide glasses [4,5]. ChGs also demonstrate lower glass transition temperatures [6] and phonon energies as compared to oxide glasses [7]. They exhibit ultrafast (~100 fs) nonlinearities, which are generally several hundred times larger than that of silica, especially for the As and Se-containing ones [8]. A vital side of ChGs physics and technology is that their properties can be conveniently shaped by variation of their composition [9 - 11].

These specific characteristics of As-, Ge- and (Ge-As)-containing ChGs and corresponding thin layers on their basis open large potential for application in fiber technologies [12], non-linear optics [13,14], for thermal

imaging systems in IR optics [15], IR lasers [16,17], chemical sensors [18,19], ion selective membranes [20-22] etc. Photoinduced effects such as photo-darkening and photocrystallization, accompanied with significant changes in the optical constants, have been applied successfully to optical recording of information [23, 24].

The design and implementation of optical components based on these materials requires detailed information on their optical properties such as optical energy gap and refractive index. Moreover, the study of the optical properties of ChGs is important for the determination of their electronic structure [25, 26, 27].

The present study is the next step of a comprehensive research, which we have undertaken for elaboration of new ChGs of the system $\text{As}_2\text{Se}_3\text{-Ag}_4\text{SSe-PbTe}$, characterized with a wide region of glass formation. Recently we have studied the phase equilibria and phase diagrams of the binary systems $\text{As}_2\text{Se}_3\text{-Ag}_4\text{SSe}$ [28], $\text{As}_2\text{Se}_3\text{-PbTe}$ [29] and $\text{Ag}_4\text{SSe-PbTe}$ [30]. The extended region of glass formation found for the three-component system $\text{As}_2\text{Se}_3\text{-Ag}_4\text{SSe-PbTe}$ [31] is in line with our prediction that the involvement of typical crystal compounds such as PbTe and Ag_4SSe in the glassy matrix of As_2Se_3 leads to its considerable enlargement. In particular, glasses containing up to 25 mol % Ag_4SSe are feasible in the system $\text{As}_2\text{Se}_3\text{-Ag}_4\text{SSe}$, while this percentage rises above 50 mol % under the introduction of

PbTe [31]. Considering that the optical properties of the amorphous chalcogenides are determined by the structural bonding between neighboring atoms, it could be expected that the introduction of Ag₄SSe and PbTe in the As₂Se₃ matrix would strongly modify these properties. Thus, widening the glass formation region which allows largely varying the composition would open the potential for tuning a desired optical parameter in a possible infrared application. Consequently, in order to optimize and fully explore the glasses from this newly synthesized system, it is worth studying the compositional dependence of their optical properties in a wide spectral range – from the UV to the near infrared.

The present paper aims at the optical characterization of bulk chalcogenide glasses from the system As₂Se₃-Ag₄SSe-PbTe and reports on new data for the optical parameters such as refractive index, absorption coefficient, optical bandgap and Urbach energies. The dependences of these parameters on glass composition are revealed and discussed.

2. Theory/calculation

The real and imaginary part of the dielectric constants ϵ_r and ϵ_i , respectively, are determined through non-linear minimization of the discrepancies between measured and calculated reflectance spectra in the spectral range of high absorption (200-1500 nm). A parametrization model of the dielectric function is used where ϵ_i is determined by multiplying the Tauc joint density of states by the ϵ_i , obtained from the Lorentz oscillator model [32, 33]. The real part of the dielectric function ϵ_r is calculated from the imaginary part using Kramers–Kronig integration [32]. Optical constants - refractive index (n) and extinction coefficient (k), are determined from the dielectric function by considering the relationships: $\epsilon_r = n^2 - k^2$ and $\epsilon_i = 2nk$. Further, the absorption coefficient α (cm⁻¹) can be easily calculated from $\alpha = 4\pi k/\lambda$, where λ is the wavelength of light. This approach has already been successfully applied to the determination of the optical properties of amorphous chalcogenide glasses [33, 34].

In the region of weak absorption ($\lambda > 1500$ nm), n and k are calculated simultaneously at each wavelength using transmittance (T) and reflectance (R) spectra along with the measured thickness (d) as inputs. For minimization of the goal function, consisting of discrepancies between measured and calculated T and R spectra, the Newton-Raphson algorithm is used [35, 36]. The error of n is 0.02, while that of k varies from 0.01 in the strong absorption region to 10⁻⁴ in the weak absorption region [35].

It is known that in amorphous ChGs the absorption coefficient ranges in three intervals [18, 37]: i) $\alpha > 10^4$ cm⁻¹; ii) $1\text{cm}^{-1} < \alpha < 10^4$ cm⁻¹ and ii) $\alpha < 1\text{cm}^{-1}$. In the first region the dependence of the absorption coefficient on the energy of light E is described by the power function:

$$\alpha \sim \frac{(E - E_g^{opt})^2}{E} \quad (1)$$

where E_g^{opt} is the width of the optical bandgap. Thus E_g^{opt} is determined by a linear fit of the so called Tauc plot: $(\alpha E)^{1/2}$ versus E , for $(\alpha E)^{1/2} = 0$. In the second region α obeys an exponential decay in the form:

$$\alpha = \alpha_0 \exp\left(-\frac{E}{E_U}\right) \quad (2)$$

where E_U , known as Urbach energy, is a measure of the structural disorder in glasses. E_U is calculated from the linear part of the plot $\ln(\alpha/\alpha_0)$ versus E . The third part of the α -spectra is outside the investigated region and is not considered in this study. The error of E_g^{opt} is 0.05 eV while that of E_U is 10 meV.

3. Materials and methods

3.1. Synthesis of glasses

The synthesis of both the starting components (As₂Se₃, Ag₄SSe and PbTe) and the studied glasses from the system As₂Se₃-Ag₄SSe-PbTe was described in details in Amova et al. [31].

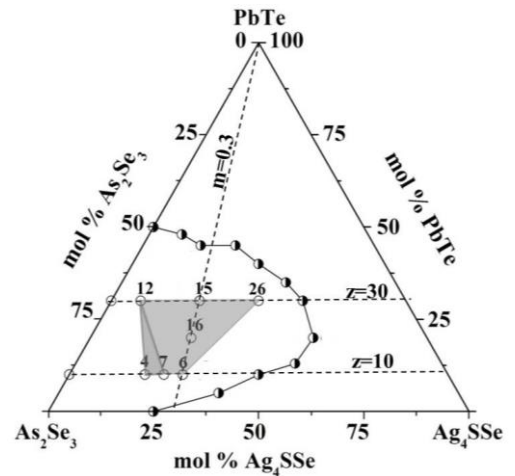


Fig. 1. Glass forming region in the system As₂Se₃-Ag₄SSe-PbTe with studied glasses denoted on the figure

Seven samples in the glass forming region (Fig. 1) were selected. This selection sets property variations in a functional dependence on two concentration parameters - z (samples 15, 16 and 6) and m (12, 15 and 26 at $z=30$, and 4, 7 and 6 at $z=10$), where z is PbTe concentration in mol %, $m=y/(x+y)$, x and y being As₂Se₃ and Ag₄SSe mol % concentrations, respectively (Table 1).

Table 1. Composition in mol %, concentration parameter $m=y/(x+y)$, calculated concentration of [Se] and [Ag+Pb] in at.% and thickness of the samples from the system $(As_2Se_3)_x(Ag_4SSe)_y(PbTe)_z$

Sample	Composition, mol %			m	Se [at %]	Ag+Pb [at %]	d , cm
	x	y	z				
s4	72	18	10	0.20	47.96	16.80	0.1339
s7	67.5	22.5	10	0.25	45.69	20.30	0.1750
s6	63	27	10	0.30	43.46	23.74	0.1800
s16	56	24	20	0.30	41.38	25.00	0.1803
s12	63	7	30	0.10	47.01	13.90	0.1329
s15	49	21	30	0.30	38.98	26.45	0.1710
s26	35	35	30	0.50	31.46	38.20	0.195

3.2. Preparation of the samples

The studied samples were cut using diamond disk in order to obtain the appropriate size and then subjected to two-step grinding with silicon carbide abrasive with 30 μm and 8 μm grain sizes, respectively. The surface was finished by polishing with CeO_2 polishing powder with particles size of 1 μm and washed with ethanol.

3.3. Measurements

Transmittance (T) and reflectance spectra (R) of the samples were measured at normal light incidence of unpolarized light using a UV-VIS-NIR spectrophotometer Cary 5E (Varian) in the spectral range 200–2500 nm with an accuracy of 0.1 and 0.3 %, respectively.

The thicknesses were measured by contact mechanical profiler with an accuracy of 10 μm . These are presented in Table 1.

The optical quality of the samples was investigated by surface imaging using an optical profiler Zeta-20 (Zeta Instruments).

4. Results

Fig. 2 presents typical two dimensional images of the surface of the studied samples taken with the optical profiler. It is seen that the samples are of approximately the same surface finishing. Despite some tiny scratches at the surface, they are well polished and homogeneous. The overall roughness (rms roughness) varies between 3 and 5 nm.

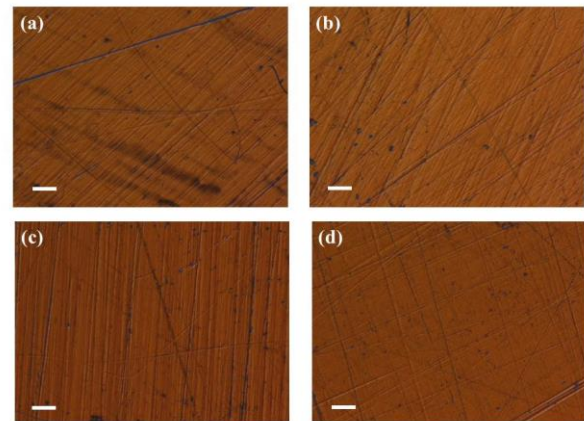


Fig. 2. Surface images of samples s4 (a), s7 (b), s12 (c) and s16 (d). The bar is 7 microns

Transmittance (T) and reflectance (R) spectra of the samples are shown in Figure 3. It is seen that for wavelength lower than 1500 nm (0.83 eV) transmittance is zero, i.e the samples are opaque. At wavelength higher than 1500 nm an increase in T is obtained although the values for s6 and s26 are zero in the whole spectral range and are not displayed in Fig. 3. Reflectance spectra of the samples (Fig. 3(b)) have a peak located in the spectral range 500 - 700 nm depending on the chemical composition of the samples.

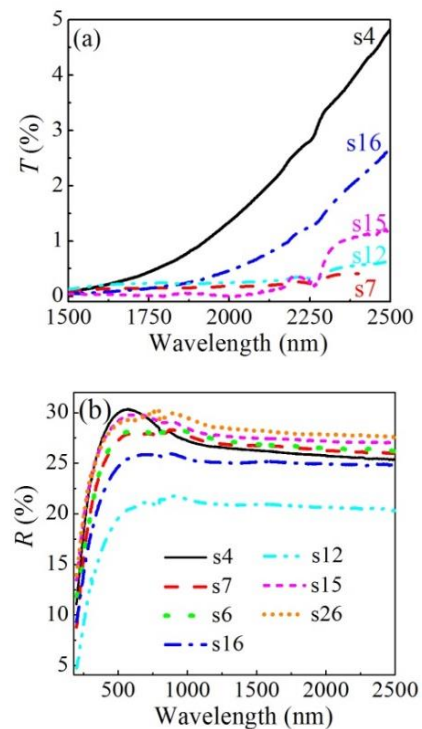


Fig. 3. Transmittance (a) and reflectance (b) spectra

Fig. 4 presents the values of the refractive index and absorption coefficient of the samples calculated using the transmittance and reflectance spectra and the models and methods described in Section 2. Refractive index varies in the range $1.5\div 3.5$ and obeys normal dispersion for wavelength higher than 650 nm and anomalous dispersion for shorter wavelengths. The values of n in the weak (2400 nm) absorption region are shown in Table 2. The spectral positions of the absorption peaks are in the range $310\div 350\text{ nm}$, depending on the glass composition. The horizontal line $\alpha = 10^4\text{ cm}^{-1}$ divides the spectral region into two regions, Tauc and Urbach regions, where optical bandgap and Urbach energies are calculated, respectively.

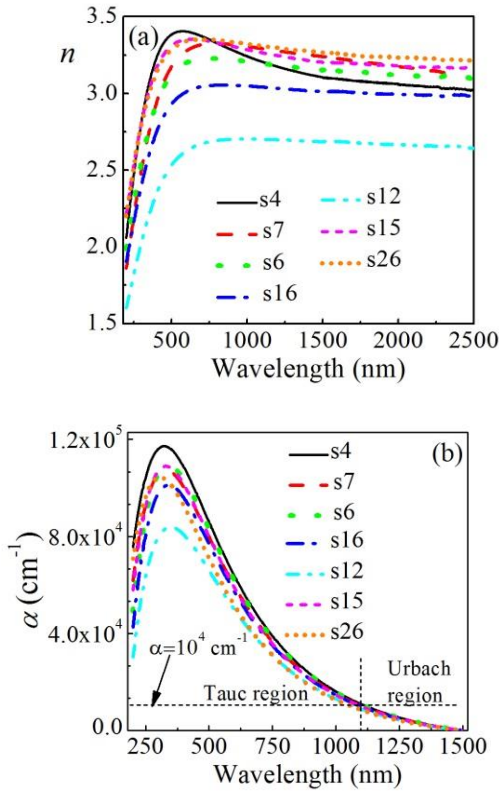


Fig. 4. Refractive index (a) and absorption coefficient (b) calculated from T and R spectra according to the models described in section 2. The horizontal and vertical dashed lines divide the spectral range to Tauc and Urbach regions where optical bandgap and Urbach energies are calculated

The already calculated values of the absorption coefficient are further used for determination of the optical bandgap and Urbach energy (Fig. 5). The samples with the highest and lowest absorption coefficients s4 and s12, respectively, are chosen for illustration. The calculated values for the optical bandgap are shown in Table 2. No sizable variation with composition is observed. The determination of E_U is illustrated by two examples in Fig. 5b. The values of E_U are determined from the slope of the linear part of the plot $\ln(\alpha/\alpha_0)$ versus E and are shown in Table 2. For all samples the values of E_U are around 220 meV with slight variation with composition.

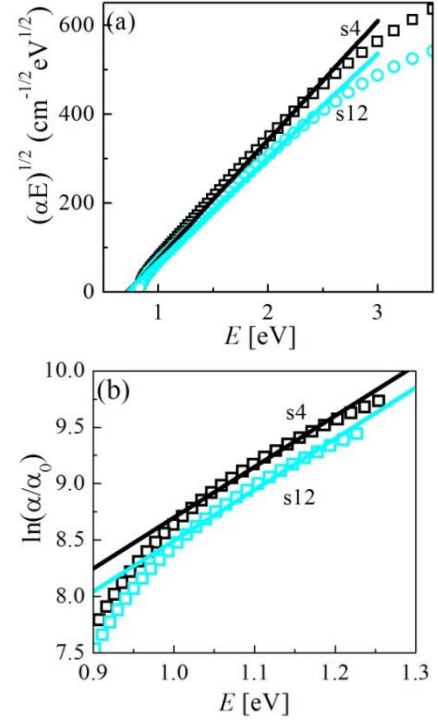


Fig. 5. Tauc plot for determination of E_g^{opt} (a) and $\ln(\alpha/\alpha_0)$ on energy dependence for Urbach energy calculation (b)

Table 2. Calculated refractive index n in the region of weak absorption (2400 nm), optical bandgap energy, E_g^{opt} , and Urbach energy, E_U

Sample	n_{2400}	E_g^{opt} [eV]	E_U [meV]
s4	3.03	0.72	222
s7	3.10	0.72	220
s6	3.11	0.72	219
s16	2.99	0.72	218
s12	2.65	0.71	219
s15	3.17	0.72	219
s26	3.22	0.73	219

5. Discussion

On the basis of the calculated values for E_g^{opt} and E_U (Table 2) we could speculate that the structural changes, originating from the addition of different structural units in the As_2Se_3 glassy matrix, compensate each other and no changes are ultimately observed. The mean value of E_U in the studied region is 219 meV , which should be related to a considerable structural disorder.

The dependences of n on the concentration parameters m and z are presented in Fig. 6. For $z=10$ the change with m is very weak, while for $z=30$ a substantial increase is

detected for $m = 0.1-0.3$ (Fig. 6(a)). Further increase of m from 0.3 to 0.5 does not lead to considerable change in n .

Taking into account that the refractive index is proportional to the electronic polarizability, which is inversely proportional to the interatomic spacing, it is clear that it correlates to samples density, so that higher n values are expected for denser samples. It was shown [31] that the density values of studied ChGs do not change significantly in the range $0.2 \leq m \leq 0.35$: at $z=10$ the density varies with m from 5.44 g/cm^3 for $m=0.2$ to 5.49 g/cm^3 for $m=0.35$. This was attributed to the presence of a phase with composition $\text{Ag}_4\text{SSe} \cdot 2\text{As}_2\text{Se}_3$ in the binary As_2Se_3 - Ag_4SSe system [31]. Therefore the close values of n obtained for 10 % mol PbTe within the interval $0.2 \leq m \leq 0.3$ (Fig. 6(a)) are due to the similarly close densities of the samples. On the contrary, at higher concentration of PbTe ($z=30$ % mol) the m -dependence of density is stronger: 5.14 g/cm^3 for $m=0.2$, 5.75 g/cm^3 for $m=0.3$ and 5.97 g/cm^3 for $m=0.5$ [31]. Thus the strong increase of n from 2.65 to 3.17, obtained for $0.1 \leq m \leq 0.3$ and $z=30$ (Fig. 6(a)), correlates well to the strong change in the density in this interval while further weaker increase from 3.17 to 3.22 relates to the density behavior for $0.3 \leq m \leq 0.5$. We can conclude that the observed dependences $n(m)$ are in line with the composition dependence of glass density [31]. Further, the $n(z)$ dependence in Fig. 6(b) displays a minimum at $z=20$ % mol.

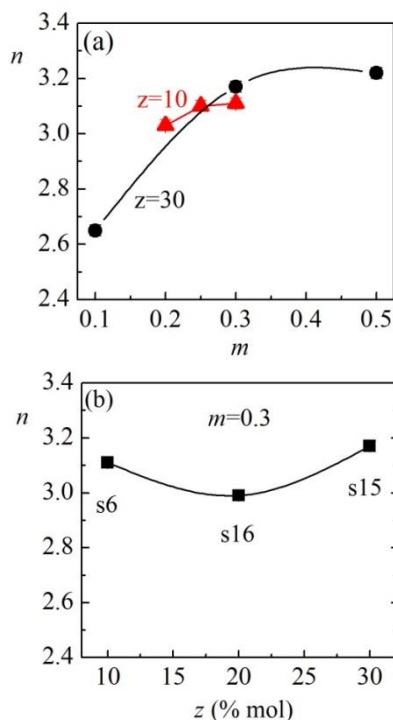


Fig. 6. Dependences of n on: a) $m=y/(x+y)$ at fixed values of $z=10$ (red triangles) and $z=30$ (black circles); b) z at $m=0.3$, where x , y and z are mol% of As_2Se_3 , Ag_4SSe and PbTe , respectively

Taking into account that the density of Ag_4SSe (7.40 g/cm^3 [28]) is higher than that of As_2Se_3 (4.54 g/cm^3 [28]), we assume that the smaller n for s16 comes from the lower

concentration of Ag_4SSe in s16 as compared to s6. The further decrease of Ag_4SSe concentration for s15 is compensated by the increase of the denser PbTe (8.16 g/cm^3 [29,30]), which finally results in an increase of the overall density and refractive index.

For further interpretation of the concentration dependences we adopt the approach of Xiang Feng et al. [38]. This relies on an excess of Se-atoms, where the chemical bonds arranging in the sequence As–Se, Pb–Se, Se–Se and Se–Te are dominant. In this case the starting components for the ChG synthesis are chemical elements, not compounds. The calculated concentrations of [Se] and [Ag+Pb] in at% are included in Table 1. Fig. 7 presents the dependence of the refractive index on the concentration of [Se].

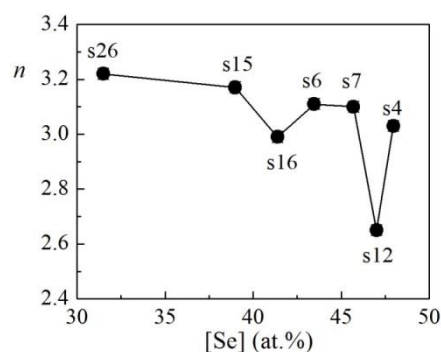


Fig. 7. Dependence of the refractive index n on the concentration of Se atoms

Generally a decrease in n is observed with increasing Se concentration with distinct minimum at [Se]=47.01 at%. The highest value (3.22) is obtained at the smallest concentration of Se atoms ([Se]=31.46 at%) and the lowest (2.65) at [Se]=47.01 at%. The abrupt structural changes in the concentration triangle ($s7 \rightarrow s12 \rightarrow s4$) (Fig. 1), associated with stepwise changes of Ag_4SSe ($22.5 \rightarrow 7 \rightarrow 18$ %) and PbTe ($10 \rightarrow 30 \rightarrow 10$ %) concentrations, determine the existence of the minimum at [Se] = 47.01 at% (s12). If the density values are considered [31], we may conclude that the densest sample is obtained for the lowest Se concentration, while the least compact one is at [Se]=47.01 at%. The appearance of the second minimum in the refractive index at [Se]=41.38 at% is reasonable since it successively involves the points $s6 \rightarrow s16 \rightarrow s15$, corresponding to $m=0.3$ and increasing concentration of PbTe in the sequence ($10 \rightarrow 20 \rightarrow 30$ mol %). We have already demonstrated that the dependence $n(z)_{m=0.3}$ has a minimum at $z=0.2$ (point s16) (Fig. 6b), which explains the minimum in $n([\text{Se}])$ at [Se]=41.38 at%.

The composition of ChG involves two heavy metals (Ag and Pb), which affect considerably the behavior of the refractive index, as seen from Fig. 8. Under increasing ([Ag]+[Pb]) n increases from 2.65 to 3.22, the dependence involving only one singular point at [Ag]+[Pb]=25.00 at. % (point s16). The comparison between Fig. 7 and Fig. 8 demonstrates that the decisive factor in obtaining high refractive index (density) is the concentration of the heavy metals.

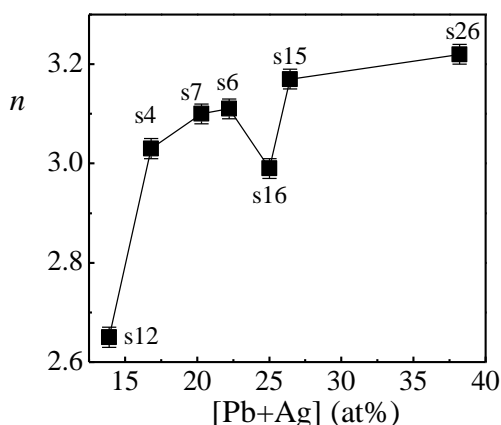


Fig. 8. Dependence of the refractive index n on the concentration of heavy metals.

6. Conclusions

Transmittance and reflectance spectra measured in the UV-VIS-NIR spectral regions along with Tauc-Lorentz parametrization model and the Newton-Raphson algorithm are successfully applied to the optical characterization of newly synthesized chalcogenide glasses from the system $(\text{As}_2\text{Se}_3)_x(\text{Ag}_4\text{SSe})_y(\text{PbTe})_z$. Refractive index, extinction coefficient, absorption coefficient, optical bandgap energy and Urbach energy are determined. The wide glass formation region of these materials allows varying the refractive index over a substantial range ($2.65 \leq n_{2400} \leq 3.22$). The variation is discussed in details in terms of glass composition and density. Peculiarity points are found and discussed also. Regarding the IR bandgap ($0.71 \leq E_g^{\text{opt}} \leq 0.73$) [eV] and the Urbach ($218 \leq E_U \leq 222$) [meV] energies, the structural changes originating from the addition of different structural units in the As_2Se_3 glassy matrix appear to compensate each other and no changes are ultimately observed.

A correlation is established between the studied optical parameters and the chalcogenide glass composition. Generally, the refractive index increases with the concentrations of PbTe, heavy metals ([Ag+Pb]) and $m=y/(x+y)$, x and y being the concentrations of As_2Se_3 and Ag_4SSe , respectively, and decreases with Se concentration. The densest glass with the highest refractive index is obtained for the Se concentration of 31.46 at% and [Ag+Pb] = 38.20 at%. The observed concentration dependences of n are in line with the previously determined composition dependence of glass density [31].

Acknowledgements

T. Babeva would like to acknowledge the project BG16 1P0003-1.2.04-0034-C0001 under Operational Programme "Development of the competitiveness of the Bulgarian Economy".

References

- [1] H. Nasu, K. Kubodera, *J. Am. Ceram. Soc.* **73**, 1794 (1990).
- [2] L. Tichy, H. Ticha, P. Nagels, R. Callaerts, R. Mertens, M. Vlcek, *Mater. Lett.* **39**, 122 (1999).
- [3] D. W. Hewak, D. Brady, R. J. Curry, G. Elliott, C. Huang, M. Hughes, K. Knight, A. Mairaj, M. Petrovich, R. Simpson, C. Smith, C. Sproat, Chalcogenide glasses for photonics device applications, in *Photonic Glasses and Glass Ceramics*, Chap. 2, Editor G.S. Murugan, Research Signpost, Kerala, India (2010).
- [4] S. Hocde, C. Boussard-Pledel, G. Fonteneau, D. Lecoq, H. L. Ma, J. Lucas, *J. Non-Cryst. Sol.* **274**, 17 (2000).
- [5] M. Fadel, *Vacuum* **52**, 277 (1999).
- [6] A. Feltz, *Amorphous Inorganic Materials and Glasses*, VCH, Weinheim (1993).
- [7] J. A. Savage, *J. Non-Cryst. Solids* **47**, 101 (1982).
- [8] C. Quémard, F. Smektala, V. Couderc, A. Barthélémy, J. Lucas, *J. Phys. Chem. Solids* **62**, 1435 (2001).
- [9] Y. Yang, Z. Yang, P. Lucas, Y. Wang, Z. Yang, A. Yang, B. Zhang, H. Tao, *J. Non-Cryst. Sol.* **440**, 38 (2016).
- [10] M. Kalyva, J. Orava, A. Siokou, M. Pavlista, T. Wagner, S. N. Yannopoulos, *Adv. Funct. Mater.* **23**, 2052 (2013).
- [11] B. Gleason, P. Wachtel, J. D. Musgraves, A. Qiao, N. Anheier, K. Richardson, *Proc. of SPIE* **8884**, 888417 (2013).
- [12] W. H. Kim, V. Q. Nguyen, L. B. Shaw, L. E. Busse, C. Florea, D. J. Gibson, R. R. Gattass, S. S. Bayya, F. H. Kung, G. D. Chin, R. E. Miklos, I. D. Aggarwal, J. S. Sanghera, *J. Non-Cryst. Sol.* **431**(1), 8 (2016).
- [13] B. J. Eggleton, B. Luther-Davies, K. Richardson, *Nat. Photonics* **5**, 141 (2011).
- [14] B. Zhang, W. Guo, Y. Yu, C. Zhai, S. Qi, A. Yang, L. Li, Z. Yang, R. Wang, D. Tang, G. Tao, B. Luther-Davies, *J. Am. Ceram. Soc.* **98**, 1389 (2015).
- [15] D. Cha, H. Kim, Y. Hwang, J. Jeong, J. Kim, *Appl. Opt.* **51**, 5649 (2012).
- [16] A. B. Seddon, Z. Q. Tang, D. Furniss, S. Sujecki, T. M. Benson, *Opt. Express* **18**, 26704 (2010).
- [17] L.B. Shaw, P.A. Thielen, J. S. Sanghera, S. S. Bayya, I. D. Aggarwal, *Proc. SPIE* **4974**, 60 (2003).
- [18] J. Charrier, M. L. Brandily, H. Lhermite, K. Michel, B. Bureau, F. Verger, V. Nazabal, *Sens. Actuat. B-Chem.* **173**, 468 (2012).
- [19] P. Ma, D. Choi, Y. Yu, X. Gai, Z. Yang, S. Debbarma, S. Madden, B. Luther-Davies, *Opt. Express* **21**, 29927 (2013).
- [20] V. Vassilev, K. Tomova, S. Boycheva, *J. Non-Cryst. Sol.* **353**, 2779 (2007).
- [21] V. Vassilev, K. Tomova, S. Boycheva, V. Parvanova, *J. Non-Cryst. Sol.* **355**, 1566 (2009).

- [22] A. Pradel, O. Walls, C. Cali, G. Taillades, A. Bratov, C. Dominguez, M. Ribes, J. Optoelectron. Adv. M. **3**, 641 (2001).
- [23] Y. Isbi, S. Sternklar, E. Granot, V. Lyubin, M. Klebanov, A. Lewis, Opt. Commun. **171**, 219 (1999).
- [24] P. Nagels, L. Tichy, E. Sleenckx, R. Callaerts, J. Non-Cryst. Solids **227-230**, 705 (1998).
- [25] H. G. Dantanarayana, A. Vukovic, P. Sewell, Z. G. Lian, D. Furniss, A. B. Seddon, E. A. Romanova, A. Konyukhov, B. Derkowska, J. Orava, T. Wagner, T. M. Benson, Transparent Optical Networks (ICTON), 2010, p. 1.
- [26] K. Sharma, M. Lal, N. Goyal, J. Optoelectronic and Biomedical Materials **6(2)**, 27 (2014).
- [27] P. Nemeč, M. Olivier, E. Baudet, A. Kalendova, P. Benda, V. Nazabal, Mat. Res. Bull., Elsevier **51**, 176 (2014).
- [28] V. Vassilev, L. Aljihmani, V. Parvanova, J. Therm. Anal. and Calorim. **85**, 309 (2006).
- [29] V. Vassilev, A. Amova, L. Aljihmani, I. Mihaylova, VIII Intern. Sci. Conf. Unitech'08, vol. III, Gabrovo, Bulgaria, 2008, p.459.
- [30] A. Amova, T. Hristova-Vasileva, V. Vassilev, Thermochem. Acta **531**, 42 (2012).
- [31] A. Amova, T. Hristova-Vasileva, L. Aljihmani, I. Bineva, V. Vassilev, J. Alloys Compd. **573**, 32 (2013).
- [32] G. E. Jellison Jr., F. A. Modine, Appl. Phys. Lett. **69**, 371 (1996).
- [33] S. Boycheva, A. K. Sytchkova, J. Bulir, C. Popov, W. Kulisch, A. Piegari, J. Non-Cryst. Sol. **353**, 1618 (2007).
- [34] D. Fanta, I. Ohlidal, M. Frumar, J. Jedelsky, Appl. Surf. Sci. **175&176**, 555 (2001).
- [35] I. Konstantinov, Tz. Babeva, S. Kitova, Appl. Opt. **37**, 4260 (1998).
- [36] F. Abeles, M. Theye, Surf. Sci. **5**, 325 (1966).
- [37] A. Zakery, S. R. Elliott, An introduction to Chalcogenide glasses, in Optical Nonlinearities in Chalcogenide Glasses and their Applications, Springer-Verlag, Berlin Heidelberg (2007).
- [38] X. Feng, H. Hu, F. Lin, Phys. Chem. Glasses **40**, 225 (1999).

*Corresponding author: babeva@iomt.bas.bg